Electronic Supplementary Material (ESI) for Energy & Environmental Science.
This journal is © The Royal Society of Chemistry 2015

Geometrically-confined favourable ion packing for high gravimetric capacitance in carbon-ionic liquid supercapacitor

Xuehang Wang[1], Haitao Zhou[1], Edel Sheridan[2], John Charles Walmsley[2], Dingding Ren[3], De Chen[1*]

Affiliations:

[1] Department of Chemical Engineering, Norwegian University of Science and Technology, Sem Sælands vei 4, 7491 Trondheim, Norway

[2] SINTEF Materials and Chemistry, 7491 Trondheim, Norway

[3] Department of Electronics and Telecommunications, Norwegian University of Science and Technology, 7491 Trondheim, Norway

*Correspondence to: E-mail: de.chen@ntnu.no

Ion-packing configuration.

As discussed in the main text, there is a single layer of adsorbed cations on the cylindrical inner surface of negatively-charged. It has been measured experimentally by AFM that the ions are ordered-packed on two-dimensional graphite.[1] Hence, the ion should be also expected to be orderly packed on the electrode surface. We propose the ion-packing configuration accordingly.

Special surface-densest packing configuration (I) is defined by the ions stacking layer by layer, the pore size of each layer adapting exactly integer number of ions (*NPL*); the second layer is rotated with a twist angle that allows it to approach the first layer as close as possible (Fig. 4 II); each layer is packed with the same configuration and forms the regular pattern along the cylindrical tube (Examples: Fig. 5 scheme A, Fig. 4 II, Fig. 5 scheme C). Several other configurations (II, III(A-C), IV) represent non-special densest packing (Example: Fig. 5 scheme B & D).

II. When $D/d_{ion} < 1.00$, no ions can access the pore and the number of adsorbed ion is 0.

III. When $1.00 < D/d_{ion} < 2.00$ (or NPL < 2), the surface-densest packing can be solved as volume-densest packing as all ions are in contact with the cylindrical inner surface.[2] Extensive simulation studies have been devoted to figuring out the volume-densest pack of spherical in cylindrical pore.[2-4] There are three different densest packing regimes in this relative pore size range, named (A) normal zigzag ($1.00 < D/d_{ion} < 1.87$), (B) single helix ($1.87 < D/d_{ion} < 1.99$) and (C) double helix ($1.99 < D/d_{ion} < 2.00$) in the range of $1.00 < D/d_{ion} < 2.00$. It is worth mentioning that the zigzag structure of ion-packing configuration has been observed theoretically by molecular dynamic calculation.[5]

IV. When the densely packed particle ring (*NPL* > 2) is slightly expanded and extra space is introduced, one stable configuration is for the extra space to be shared among all the particles

equally within the same layer.[6] We suppose the same stable configuration each layer to solve the ion stacking when NPL > 2 or $D/d_{ion} > 2.00$ (Fig. 5 scheme D). *NPL* will always be an integer based on this configuration. Each layer will be the same configuration as the first layer, and only rotate a twist angle approaching each other as close as possible.

Model derivation.

Based on the ion-packing configuration, the number of adsorbed ions N (effective ion size is d_{ion}) in the pore with pore size D and pore length l can be solved as:

$$N = \frac{3D^2 \cdot l \cdot \varphi}{16 d_{ion}{}^3} \tag{S1}$$

Here φ is the volume fraction (φ = the total volume of the adsorbed ions/the volume of the pore).

1. For $1.87 < D/d_{ion} < 2.00$ (Configuration III-B and III-C), the value of φ can be directly obtained from the literature according the volume-densest packing.[2-4]

2. For $1.00 \leq D/d_{ion} < 1.87$ and $D/d_{ion} \geq 2.00$ (Configuration I, III-A and IV), some values of φ are unknown for the surface-densest packing. The number of adsorbed ions can also be solved based on the characteristics of the ion packing configurations, as:

$$N = \frac{NPL \cdot l}{Z} \tag{S2}$$

where, *NPL* is the number of ions in each layer and Z is the distance between adjacent layers:

$$NPL = \begin{cases} 1 & \text{when } 1.00 \leq D/d_{ion} < 1.87 \quad \text{(S3)} \\ n\ (n = 2, 3, 4, 5\ldots) & \text{when } \dfrac{1}{\sin(\frac{360^\circ}{2n})} + 1 \leq D/d_{ion} < \dfrac{1}{\sin(\frac{360^\circ}{2(n+1)})} + 1 \quad \text{(S4)} \end{cases}$$

$$Z = \begin{cases} (2Dd_{ion} - D^2)^{\frac{1}{2}} & \text{when } 1.00 \leq D/d_{ion} < 1.87 \quad \text{(S5)} \\ \left[d_{ion}{}^2 - \frac{1}{4}(\cos(\frac{360^\circ}{2n}) - 1)^2 \cdot (D - d_{ion})^2 - \frac{1}{4}\sin(\frac{360^\circ}{2n})^2 \cdot (D - d_{ion})^2 \right]^{\frac{1}{2}} & \text{(S6)} \\ & \text{when } D/d_{ion} \geq 2.00 \end{cases}$$

To calculate the total ions adsorbed on the surface of the material, the PSD should be taken into consideration. According to the pore length distribution curve (Fig. S5) derive by Eq. 4, the pore length l is correlated to the pore diameter D_i. The parameters φ, NPL and Z and hence N are all functions of the pore size and the effective ion size. The number of ions adsorbed on the surface of the porous material (or N_{total}) can be calculated by summing up the number of ions stored in all the ion-accessible pores (D_1 to D_i from the PSD) on the sample:

$$N_{total} = \sum_{d_{ion}}^{D_i} N\left(D_i,\ d_{ion}\right) \qquad (i = 1, 2, 3, 4\ldots \text{ and } D_0 = d_{\text{ion}}) \tag{S7}$$

Additionally, the calculated capacitances contributed from the pores larger than 10 nm is small (< 5 F/g) in this work, which could be ignored compared to the pores between d_{ion} and 10 nm.

As the discharge curve at room temperature is very close to linear, the estimated gravimetric capacitance of a single electrode can be expressed as:

$$C'_{sp,electrode} = \frac{Q}{U} = \frac{2e \cdot N_{total}}{U} \tag{S8}$$

where Q is the total charge on the electrode, U is the potential absolute value of the single electrode, which is approximately 2 V, and e is one electron charge equals to 1.6×10^{-19} C.

We generate a more general formula by combining Eq. S3-S6 with Eq. S2 to express the number of ions adsorbed in the pore with pore diameter D_i:

$$N(D_i, d_{ion}) = NLP(D_i, d_{ion}) \cdot \frac{V(D_i)}{Z(D_i, d_{ion}) \cdot \left(\pi\left(\frac{D_i}{2}\right)^2\right)} \tag{S9}$$

Here, $V(D_i)$ is the pore volume of the pore with pore diameter of D_i. We define an ion-packing function as following:

$$f(D_i, d_{ion}) = \cdot \frac{NLP(D_i, d_{ion})}{Z(D_i, d_{ion}) \cdot \left(\pi\left(\frac{D_i}{2}\right)^2\right)} \tag{S10}$$

Then, Eq. S9 is simplified into:

$$N(D_i, d_{ion}) = f(D_i, d_{ion}) \cdot V(D_i) \tag{S11}$$

However, the ion packing function is a complex function of pore size and effective ion size, which could further be derived using the term volume fraction φ.

As Eq. S1 is a general formula for evaluating N, we combined Eq. S1 and Eq. S9 and found that the volume fraction φ is a function of relative pore size (D_i/d_{ion}). Based on the definition of φ, the φ can be expressed as:

$$\varphi(D_i / d_{ion}) = \frac{volume_{allions}}{volume_{pore}} = \frac{N(D_i, d_{ion}) \cdot d_{ion}^{\ 3}}{6V(D_i)} \tag{S12}$$

The number of ions adsorbed in the pore with pore diameter D_i can be expressed by rearranging Eq. S12 as:

$$N\left(D_i, d_{ion}\right) = \frac{6V(D_i) \cdot \varphi(D_i / d_{ion})}{d_{ion}^{\ 3}} \tag{S13}$$

Comparing Eq. S13 with Eq. S11, we find the ion packing function can also be expressed by:

$$f(D_i, d_{ion}) = \frac{\varphi(D_i / d_{ion})}{d_{ion}^{\ 3}} \tag{S14}$$

Thus, a more general and simpler expression of the total number adsorbed in the pore with pore diameter D_i is given by:

$$N\left(D_i, d_{ion}\right) = V(D_i) \cdot f(\varphi(D_i / d_{ion}), d_{ion}) \tag{S15}$$

Combining Eq. S15 further with the Eq. S7, we derived the Eq. 5.

To analyze the effect of ion-packing function alone, we assume that only single pore size of D exists in the carbon material with constant pore volume V. The total ions adsorbed N_{total} is given as:

$$N_{total} = \frac{6V \cdot \varphi(D / d_{ion})}{d_{ion}^{\ 3}} \tag{S16}$$

Assuming V = 1.5 cm^3/g based on the experimental pore volume of CNS1 between the pore diameter of 1-10 nm (Table S1). The theoretical specific capacitance with monotonic PSD the can be calculated, as plotted in Fig. 5.

Temperature influence on the d_{ion}. As described in the main text, the effective ion size represents the occupation of the ions on the surface of electrode. Bjerrum length is used to describe the distance between two equal elementary charges where the electrostatic interaction between them is equal to the thermal energy. Based on the definition of the Bjerrum length with one added constant C to compensate for the impact from the electrode surface, the definition of the effective ion size is expected to be:

$$d_{ion} = \frac{e^2}{4\pi\varepsilon_0\varepsilon_r k_B T} - C \tag{S17}$$

where e is the electron charge, ε_0 is the permittivity of free space, ε_r is the relative permittivity, k_B is the Boltzmann constant and T is the absolute temperature. The relative permittivity is barely changed as the temperature increases from 20 to 60 ^oC for $EMIMBF_4$[7], and it can be regarded as a constant in this temperature range. Thus, the d_{ion} reduces with increasing temperature following Eq. S17.

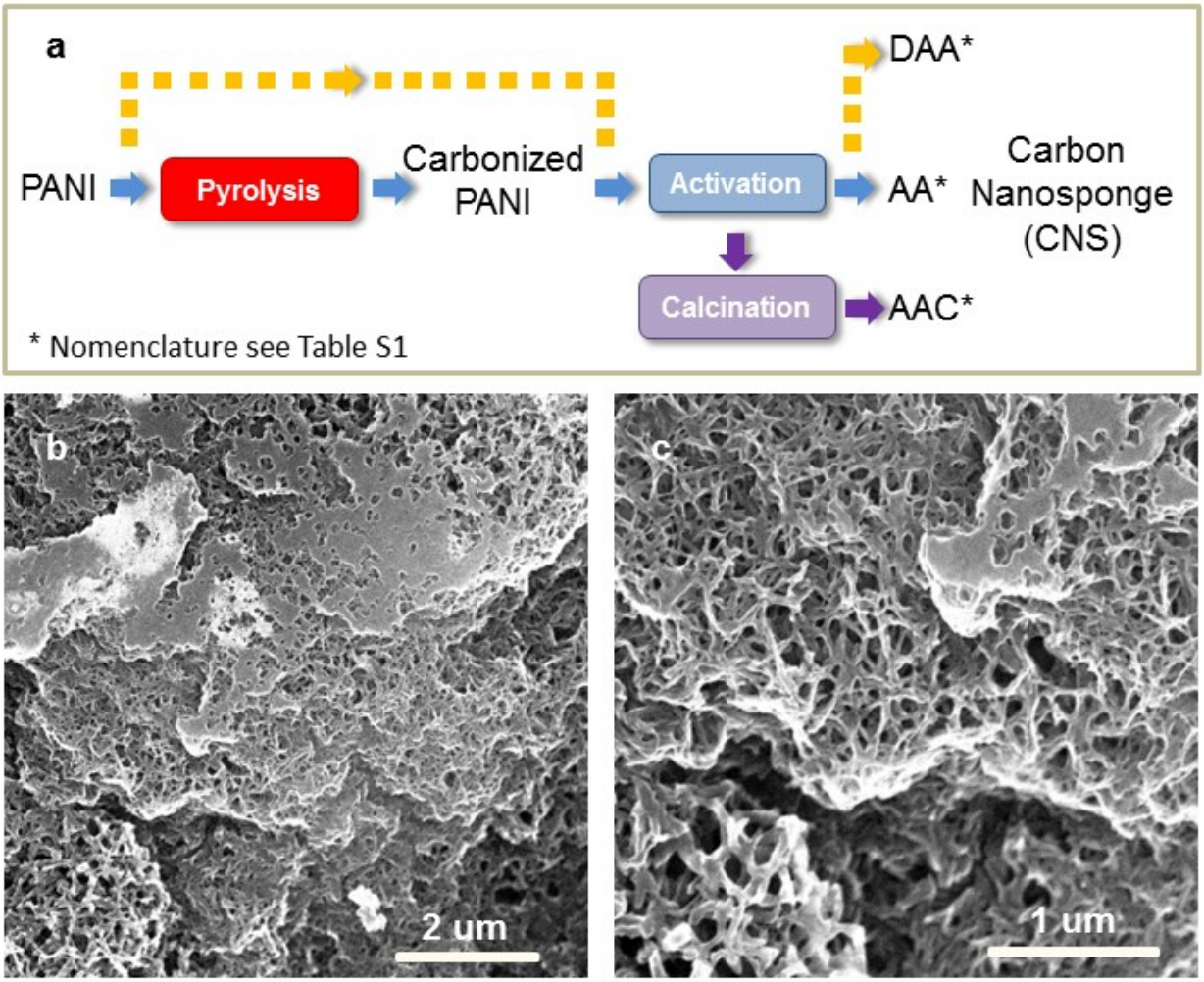

Fig. S1 (a) Schematic showing the preparation method for the CNSs. (b & c) Low magnifications SEM images of sample CNS1

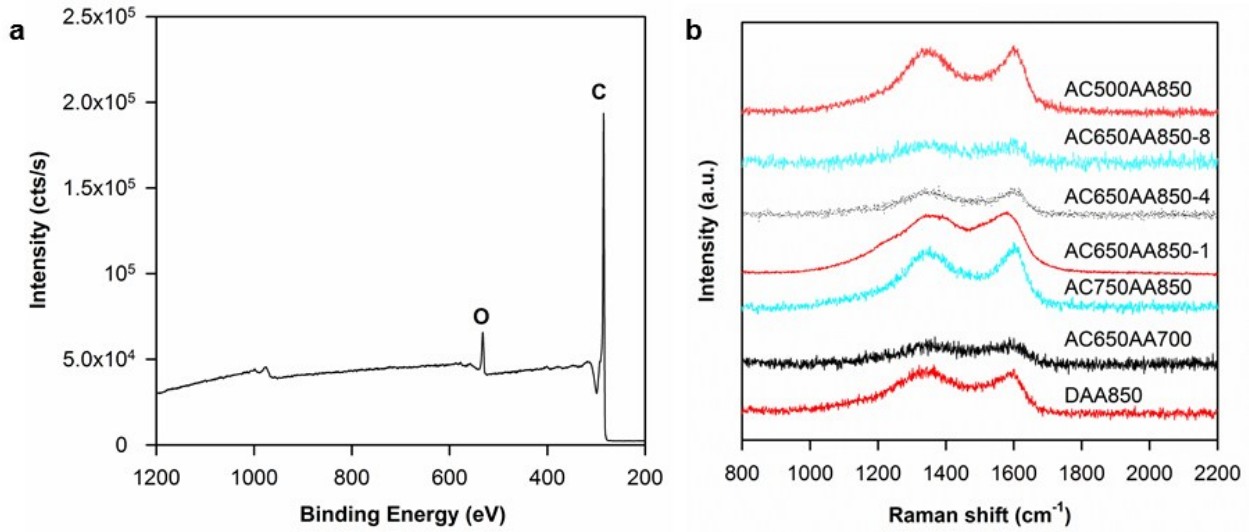

Fig. S2 (a) The XPS spectra of the samples CNS1: No obvious K2p peak (< 0.1 atomic %) was observed in XPS spectra, indicating the potassium species were almost completely removed. The presence of oxygen group (3.8-7.9 atomic %) may attribute to the small pseudo-capacitance in the CV curves (see low scan rate of CV curves in Fig. S3c & S7b).[8] We used high temperature (900 ^{o}C) to treat two of our sample to reduce the oxygen content to lower than 1 atomic %. The capacitances of both these two samples were higher than the sample without heat treatment. In addition, the capacitances of the sample after calcination still can be estimated well by our ion-packing model combining their pore size distribution (Table S1). Hence, the pseudo-capacitance due to the oxygen group contributed little compared to the total specific capacitance, and in this work, we only focus on the electrical double layer capacitive effect. (b) The Raman spectra for CNSs. Deconvolution of Raman spectrum using Lorenzian fitting shows all the I_D /I_G ratios are between 1.0-1.1, indicating the disorder in CNSs are similar.

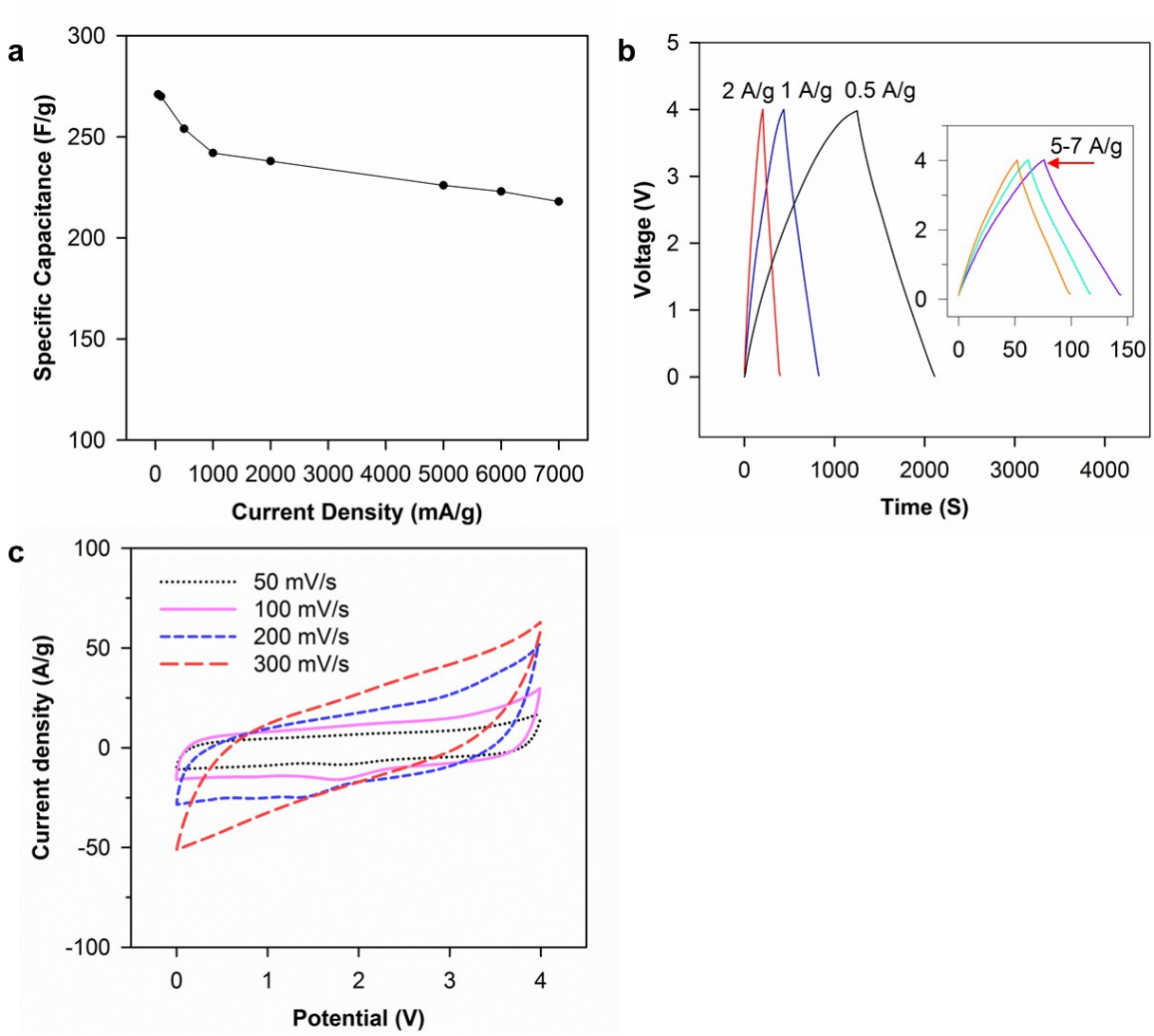

Fig. S3 Room temperature SC performance of CNS1. (a) Specific capacitance (F/g) *vs*. current density (mA/g). (b) GCD curve tested by coffee-bag cell at current densities of 0.5, 1 and 2 A/g and inset is at current densities of 5, 6 and 7 A/g. The SC with CNS1 sample delivered a high specific discharge capacitance of 254 F/g at 0.5 A/g (based on the mass loading of carbon sponge on single electrode). The SC shows good rate capability, delivering a discharge capacitance of 226 F/g at 5 A/g, which is 84 % of the value obtained at 0.1 A/g. The capacitance retention is even better than the SCs using graphene as electrode active material in the coffee-bag cell.[9] Moreover, the voltage drop (IR drop) caused by the inner resistance of the SC was barely observed at low current values. At high current density of 5-7 A/g, the SC with CNS1 sample shows only a potential drop of 0.1 V. (c) CV curve of CNS1 in neat $EMIMBF_4$: the rectangular curves from 0 to 4 V over the wide range of scan rates indicate a near-ideal capacitive behavior with good rate performance.

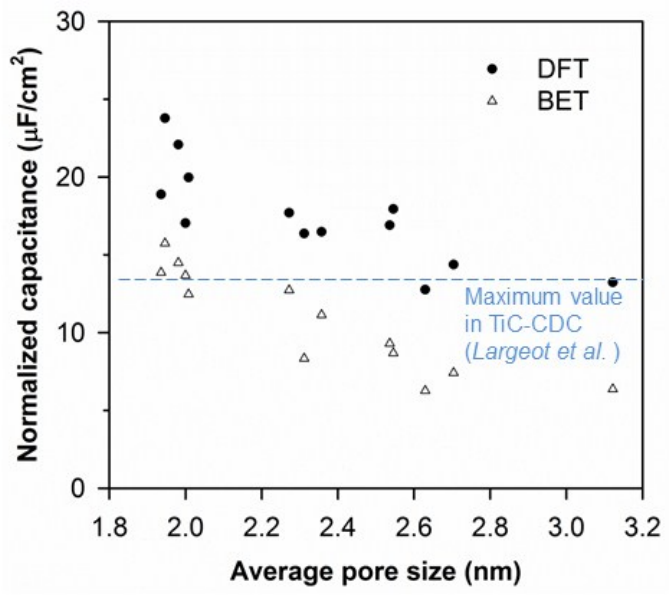

Fig. S4 Specific capacitances normalized by ion-accessible DFT SSA and BET SSA as a function of the average pore size for the CNSs in this study. As the average pore sizes are all larger than 1.9 nm, there are more mesopores than micropores in CNSs. Some of the normalized capacitance of CNSs are higher than the maximum normalized capacitance (BET) in micropore-only titanium carbide-derived carbon (TiC-CDC) of 13.5 μF/cm^2 (dash line)[10]. This is due to the presence of the pores distributed in the capacitance-detrimental region (region III in Fig. 5) for the sample with highest normalized capacitance. The TIC-CDC with very narrow PSD width (1 nm) cannot avoid the presence of the capacitance-detrimental pores, which further demonstrates the advantages of the mesoporous-capacitance-favorite region (region IV in Fig. 5).

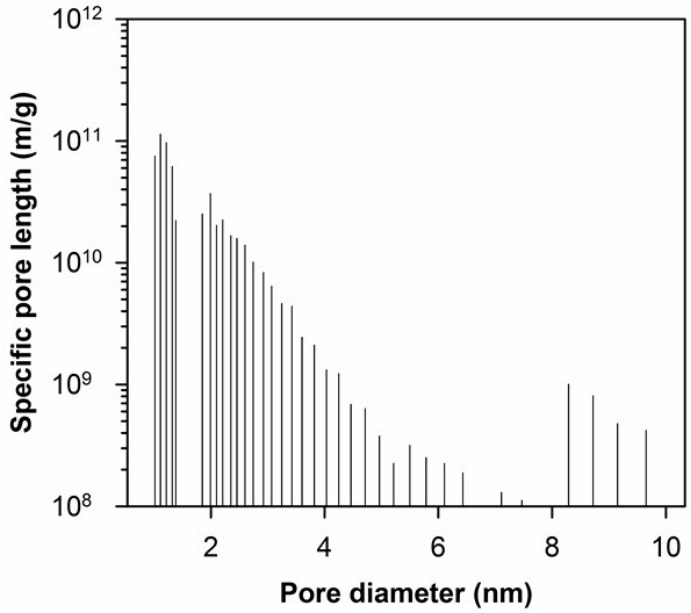

Fig. S5 Pore length distribution of CNS1 converted from accumulated pore volume curve or PSD curve in Fig. 2b based on Eq. 4.

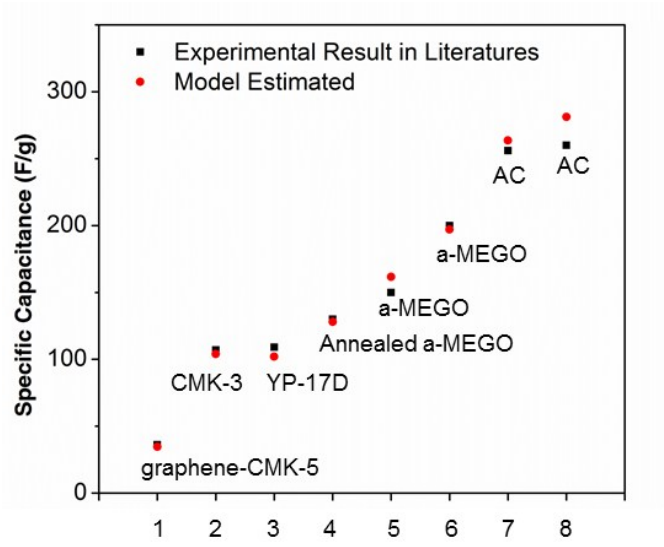

Fig. S6 Comparison between the experimental capacitance in the literature and the estimated capacitance based on our model using PSD in literature values: Black squares are experimental capacitance, from left to right, graphene-CMK-5 (Z Lei *et al*.)[11], ordered mesoporous carbon CMK-3-BET800 (ACS Material, used as the active material of the electrode, fabricated and tested in our lab using the same method as described in the Methods section , in neat $BMIMPF_6$ electrolyte, 20 ^oC, 100 mA/g), YP-17D a commercial activated carbon, the SC performance in $EMIMBF_4$ is tested by M Rose *et al*.)[12], annealed activated graphene (WY Tsai *et al*.)[13], activated graphene (WY Tsai *et al*.)[13], activated graphene (Y Zhu *et al*.)[14], Polypyrrole-derived activated carbon (AC) activated at 650 and 700 ^oC respectively (L Wei *et al*.)[15]; Red dots are estimated capacitance based on our model. The consistency of the theoretical and experimental capacitance shows the universality of the model to other porous carbon materials.

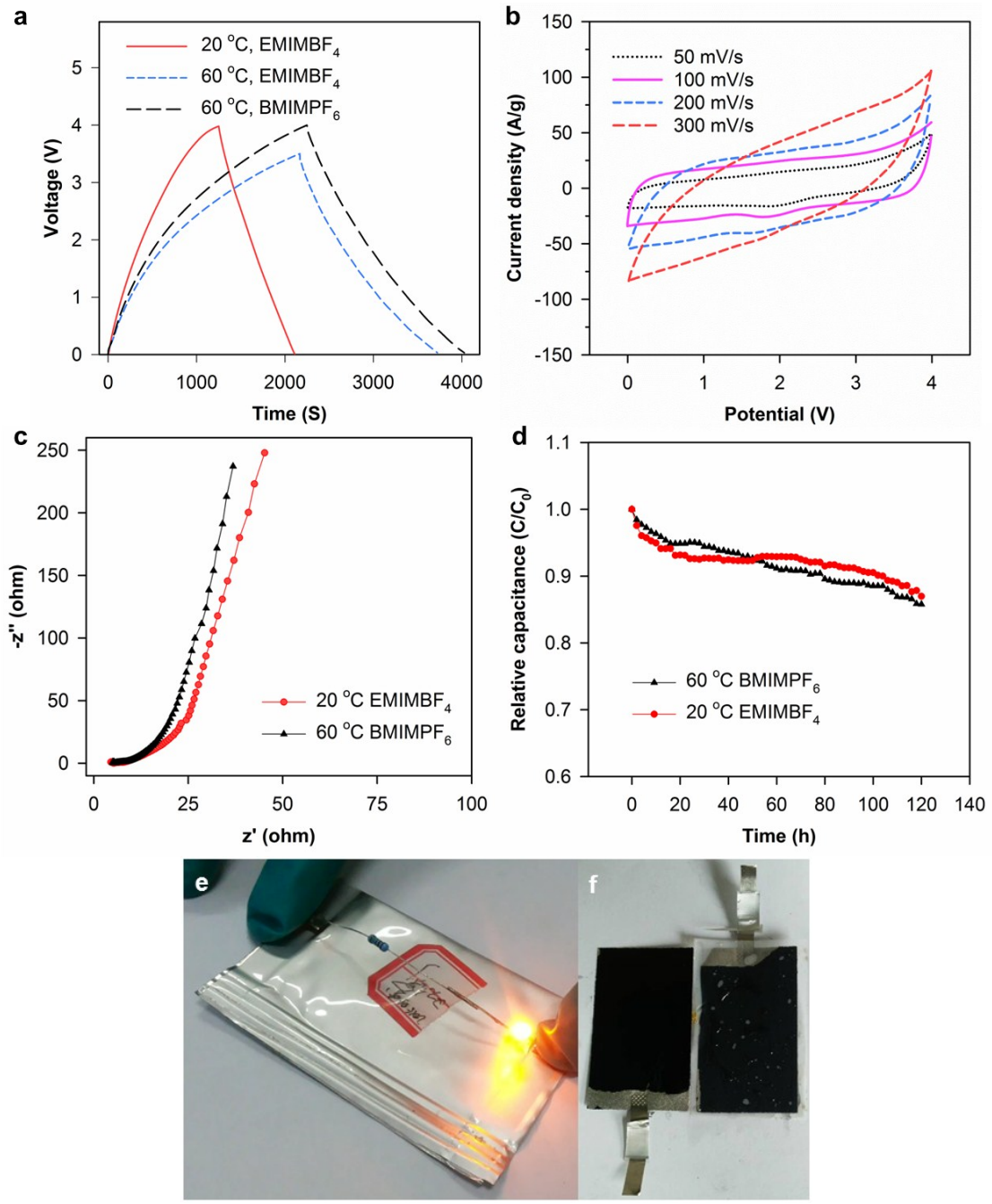

Fig. S7 (a) GCD curve recorded at the constant current density of 0.5 A/g. (b) CV curve: rectangular shape under a wide range of scan rates at 60 °C in $BMIMPF_6$. (c) The Nyquist plots (10 kHz and 100 mHz) show typical vertical curves in the low frequency region indicating a near-ideal capacitive behavior of SCs. (d) Floating test result. 89 % and 87 % of the primary capacitance was remained after 120 hours floating for $EMIMBF_4$ (20 °C) and $BMIMPF_6$ (60 °C) respectively. (e & f) The photographs of the "coffee-bag" cell and its electrodes using CNS1 as the active material. The specific capacitance was 270 F/g (100 mA/g, 20 °C) and 394 F/g (500 mA/g, 60 °C) in $EMIMBF_4$ electrolyte.

Table S1 Sample properties in this work: surface area, pore characteristics and SC performance.

Sample Code	BET SSA (m^2/g)	1-10 nm DFT ave. (cylinder) pore diameter (nm)	Width of the PSD (> 1 nm) (nm)	1-10 nm pore volume (cm^3/g)	[b]$C_{sp,electrode\ 1}$ at 0.1 A/g (F/g)	[c]$C_{sp,electrode\ 2}$
[a]AC650AA850-1	3464	2.63	6.0	1.55	212.7	211.7
AA650AA850-2	3200	3.12	6.9	1.85	220.1	220.2
AA650AA850-3	2911	2.70	6.7	1.96	196.8	194.9
AA650AA850-4 (CNS1)	3060	2.55	6.0	1.50	268.2	262.9
AA650AA850-5	2903	2.31	6.9	1.46	225.3	226.1
AA650AA850-6	3242	2.53	6.4	1.51	257.4	255.9
AA650AA850-7	2247	1.95	6.5	1.07	181.2	180.6
AA650AA850-8	2785	2.01	6.9	1.49	219.5	217.6
AA650AA850-7C	2680	1.98	7.1	1.29	213.5	210.2
AA650AA850-5C	3012	2.27	6.9	1.56	290.1	289.3
AC500AA850	2073	2.00	6.1	0.85	160.4	154.3
AC750AA850	2279	1.90	6.9	0.97	121.8	116.4
AC650AA700	2582	1.94	5.8	1.22	181.5	179.9
DAA850	3190	2.36	6.8	1.60	261.0	254.1

[a] Nomenclature AC-AA-DAA-C (AC: after heat treatment or carbonization; AA: after activation; DAA: directly activated from PANI without carbonization step; C: further calcination after activation at 900 ^oC; 1-3: activation time is 120 min; 4-7: activation time is 60 min; 8: activation time is 30 min)

[b] The capacitance is calculated based on discharge time from V_{max} to 0 on the charge/discharge curve. When we calculate the theoretical value based on the ion-packing model, we estimated the total adsorbed ions N_{total} (Eq. S7) based on the pore size distribution of the material. Then, the N_{totol} was used to calculate the electrode-stored charges Q. As the discharge curve at room temperature is very close to linear, we estimated the theoretical capacitance based on $C'_{sp}=Q/U$ (Eq. S8). The electrode-stored charges will all release with the constant current during the discharge, and the stored charges should equal to the released charges. Thus, we use the capacitance calculated by Eq. 1 (V_{max} to 0) when we compare the experimental capacitance with the theoretical estimated value.

[c] The capacitance is calculated based on discharge time from V_{max} to $V_{max}/2$ on the charge/discharge curve.

Supplementary reference

1. A. Elbourne, S. McDonald, K. Voïchovsky, F. Endres, G. G. Warr and R. Atkin, *ACS Nano*, 2015, **9**, 7608-7620.
2. A. Mughal, H. Chan, D. Weaire and S. Hutzler, *Phys. Rev. E*, 2012, **85**, 051305.
3. M. Hodak and L. Girifalco, *Phys. Rev. B*, 2003, **67**, 075419.
4. A. Mughal, H. K. Chan and D. Weaire, *Phys. Rev. Lett.*, 2011, **106**, 115704.
5. Y. Shim and H. J. Kim, *ACS Nano*, 2010, **4**, 2345-2355.
6. D. Wood, C. Santangelo and A. Dinsmore, *Soft Matter*, 2013, **9**, 10016-10024.
7. A. Göllei and A. Magyar, *Hung. J. Ind. Chem*, 2013, **41**, 11-15.
8. Y. Chen, X. Zhang, D. Zhang, P. Yu and Y. Ma, *Carbon*, 2011, **49**, 573-580.
9. Y. Xu, Z. Lin, X. Zhong, X. Huang, N. O. Weiss, Y. Huang and X. Duan, *Nat. Commun.*, 2014, **5**.
10. C. Largeot, C. Portet, J. Chmiola, P.-L. Taberna, Y. Gogotsi and P. Simon, *J. Am. Chem. Soc.*, 2008, **130**, 2730-2731.
11. Z. Lei, Z. Liu, H. Wang, X. Sun, L. Lu and X. Zhao, *J. Mater. Chem. A*, 2013, **1**, 2313-2321.
12. M. Rose, Y. Korenblit, E. Kockrick, L. Borchardt, M. Oschatz, S. Kaskel and G. Yushin, *Small*, 2011, **7**, 1108-1117.
13. W.-Y. Tsai, R. Lin, S. Murali, L. L. Zhang, J. K. McDonough, R. S. Ruoff, P.-L. Taberna, Y. Gogotsi and P. Simon, *Nano Energy*, 2013, **2**, 403-411.
14. Y. Zhu, S. Murali, M. D. Stoller, K. Ganesh, W. Cai, P. J. Ferreira, A. Pirkle, R. M. Wallace, K. A. Cychosz and M. Thommes, *Science*, 2011, **332**, 1537-1541.
15. L. Wei, M. Sevilla, A. B. Fuertes, R. Mokaya and G. Yushin, *Adv. Funct. Mater.*, 2012, **22**, 827-834.